Bulk viscosity of CO$_2$ from Rayleigh-Brillouin light scattering spectroscopy at 532 nm

Wang, Yuanqing; Ubachs, Wim; Van De Water, Willem

Important note
To cite this publication, please use the final published version (if applicable).
Please check the document version above.

Bulk viscosity of CO$_2$ from Rayleigh-Brillouin light scattering spectroscopy at 532 nm

Yuanqing Wang (iD), Wim Ubachs (iD), and Willem van de Water

View Online   Export Citation   CrossMark

ARTICLES YOU MAY BE INTERESTED IN

AIP Publishing

Bulk viscosity of CO_2 from Rayleigh-Brillouin light scattering spectroscopy at 532 nm

View Online   Export Citation   CrossMark

Yuanqing Wang,[1] Wim Ubachs,[1,a] and Willem van de Water[2]

AFFILIATIONS

[1] Department of Physics and Astronomy, LaserLaB, Vrije Universiteit, De Boelelaan 1081, 1081 HV Amsterdam, The Netherlands
[2] Laboratory for Aero and Hydrodynamics, Faculty of Mechanical, Maritime and Materials Engineering,
  Delft University of Technology, Leeghwaterstraat 29, 2628CB Delft, The Netherlands

[a] Electronic mail: w.m.g.ubachs@vu.nl

ABSTRACT

Rayleigh-Brillouin scattering spectra of CO_2 were measured at pressures ranging from 0.5 to 4 bars and temperatures from 257 to 355 K using green laser light (wavelength 532 nm, scattering angle of 55.7°). These spectra were compared to two line shape models, which take the bulk viscosity as a parameter. One model applies to the kinetic regime, i.e., low pressures, while the second model uses the continuum, hydrodynamic approach and takes the rotational relaxation time as a parameter, which translates into the bulk viscosity. We do not find a significant dependence of the bulk viscosity with pressure or temperature. At pressures where both models apply, we find a consistent value of the ratio of bulk viscosity over shear viscosity $\eta_b/\eta_s = 0.41 \pm 0.10$. This value is four orders of magnitude smaller than the common value that is based on the damping of ultrasound and signifies that in light scattering only relaxation of rotational modes matters, while vibrational modes remain "frozen."

Published under license by AIP Publishing. https://doi.org/10.1063/1.5093541

I. INTRODUCTION

The light scattering properties of carbon dioxide remain of interest, both from a fundamental perspective studying the relaxation in molecular gases and for determining their thermodynamic properties, as well as from an applied perspective. Details of Rayleigh-Brillouin (RB) phenomena, scattering spectral profiles of CO_2 gas at differing pressures and temperatures,[1–3] as well as its cross section,[4] are of relevance for current and future remote sensing exploration of the planetary atmospheres where CO_2 is the main constituent, either under high-pressure and high-temperature conditions as on Venus[5] or under low pressure and low-temperature conditions as on Mars.[6] The fact that carbon dioxide is the prime greenhouse gas has spurred large-scale activity in the transformation of this gaseous species,[7,8] through catalytic hydrogenation,[9] and electrochemical conversion into renewable energy,[10] as well as in plasma-driven dissociation for the synthesis of fuel from CO_2.[11,12] Apart from issues of capture, fixation, and transformation of teratons of carbon dioxide, its storage and transport, either in the liquid or gas phase, forms an important challenge.[13,14] For these purposes, the study of the transport coefficients of CO_2 gas, such as

thermal conductivity,[15] heat capacity, and shear viscosity,[16,17] is of practical importance. Light scattering is an elegant way to determine the thermodynamic properties of a gas because the Rayleigh scattering phenomenon resulting in the elastic peak is connected to entropy fluctuations,[18] while the Brillouin-side peaks are associated with density fluctuations or sound.[19,20] The macroscopic gas transport coefficients govern the scattering spectral profiles and can in turn be deduced from the measurement of such profiles.[21] This holds for both spontaneous RB-scattering[22–24] and coherent RB-scattering.[25,26]

The bulk viscosity, η_b,[27,28] is the most elusive transport coefficient. It is associated with the relaxation of internal degrees of freedom of the molecule, i.e., rotations and vibrations. The bulk viscosity is commonly measured from the damping of ultrasound at frequencies in the megahertz domain.[29] It can also be retrieved from the light scattering spectrum of molecular gases. This was demonstrated by Pan et al.[2] and recently for N_2, O_2, and air by Gu and Ubachs[30] and for N_2O gas by Wang et al.[31] In light scattering, the frequencies f_s involved are those of sound with wavelengths comparable to that of light, three orders of magnitude larger than the frequencies used to measure η_b from ultrasound experiments. The bulk viscosity of CO_2

from light scattering is found to be four orders of magnitude smaller than that from ultrasound experiments.[1–3] A simple explanation is that at high (hypersound) frequencies the relaxation of vibrational modes of the CO_2 molecule no longer plays a role, i.e., the vibrational energy stays frozen in.

The bulk viscosity can be expressed in terms of relaxation times of intramolecular degrees of freedom

$$\eta_b = p \frac{2}{(3 + \sum_i N_i)^2} \sum_i N_i \tau_i, \qquad (1)$$

where p is the pressure, N_i is the number of degrees of freedom of mode i (rotations, vibrations), and τ_i is the relaxation time (τ_{rot}, τ_{vib}).[32] A frequency-dependent version of this formula, depending on the product $f_s \tau_i$, was given by Meijer et al.[26] Carbon dioxide is a linear molecule with 2 rotational degrees of freedom. In the case of frozen vibrations ($f_s \tau_{vib} \gg 1$), Eq. (1) reduces to

$$\eta_b = \frac{4}{25} p \, \tau_{rot}. \qquad (2)$$

The vibrational relaxation time strongly decreases with temperature, and so does the bulk viscosity. In a simple model, Landau and Teller proposed an exponential dependence of the chance of relaxation on the ratio of the collision interaction time and the vibration period.[29] This leads to a scaling prediction for the temperature dependence of the bulk viscosity which agrees with the experiment.[27] On the other hand, a classical analysis of collisions of rigid rotators by Parker[33] results in a scaling expression for τ_{rot} which predicts an "increase" in τ_{rot} with increasing temperature.

The bulk viscosity changes with temperature motivated the present study in which laser-based light scattering measurements in CO_2 gas are carried out in a pressure regime of 0.5–4 bars and in a temperature regime of 257–355 K. Accurate, highly spectrally resolved and high signal-to-noise scattering line profiles are measured at a scattering angle of 55.7° and a scattering wavelength of λ_i = 532 nm, a wavelength commonly used in Lidar applications. Under these conditions of a longer wavelength and a smaller scattering angle than in a previous study,[3] the Brillouin-side peaks become more pronounced in the scattering spectrum.

Experimental data are analyzed in the context of two models for the spectral line shape. One model applies at low pressures, the kinetic regime where the mean free path between collisions is comparable to the wavelength of light,[34,35] while the other one is valid in the hydrodynamic regime.[36] Values of the bulk viscosity are determined using a least squares method by comparing model spectra to the measured ones.

The remainder of this article consists of an experimental section, a section discussing the bulk viscosity and model descriptions for RB-scattering, a presentation of results in the context of applicable models to describe the scattering spectrum, followed by a conclusion.

II. EXPERIMENT

The experimental apparatus for measuring the RB-scattering spectral profiles of CO_2 is displayed in Fig. 1. The laser source provides continuous wave radiation at λ_i = 532.22 nm at a bandwidth of less than 5 MHz. RB-scattered light is produced from the laser beam of 5 W intensity traversing a gas cell equipped with a gas inlet valve and a pressure sensor. Brewster-angled windows are mounted at the entrance and exit ports, and black paint covers the inside walls, to reduce unwanted scatter contributions. A temperature control system equipped with Peltier elements is employed for heating, cooling, and keeping the cell at a constant temperature with uncertainty less than 0.1 °C. RB-scattered light is captured at a scattering angle $\theta = (55.7 \pm 0.3)°$ defined by the setting of a slit in the scatter beam path (see Fig. 1), which also limits the opening angle for collecting RB-scattered light to less than 0.5°. The exact scatter angle and uncertainty are determined with
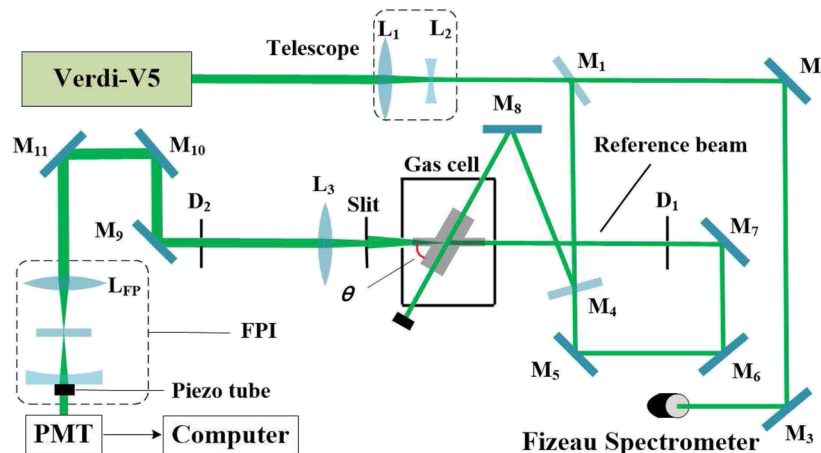
FIG. 1. Schematic of the experimental apparatus. A Verdi-V5 laser provides continuous wave light at 532.22 nm at a power of 5 W and a bandwidth less than 5 MHz. The laser light is split into two beams: The pump beam crosses the RB-scattering gas cell producing scattered light that is captured under an angle $\theta = (55.7 \pm 0.3)°$. The small fraction reference beam transmitted through M_1 is used to align the beam path after the gas cell toward the detector. The scattered light is analyzed in a Fabry-Pérot Interferometer (FPI), with a free spectral range of 2.9964 GHz and an instrument linewidth of (58 ± 3) MHz, and is collected on a photomultiplier tube (PMT). Mirrors, lenses, and diaphragm pinholes are indicated as M_i, L_i, and D_i, respectively. A slit of 500 μm is inserted to limit the opening angle for collected scattering light, therewith optimizing the resolution.

FIG. 2. (a) Experimental data for the RB-light scattering spectrum of CO_2 measured at λ_i = 532 nm, θ = 55.7°, and (p,T) conditions as indicated, corresponding to a uniformity parameter y = 1.88; 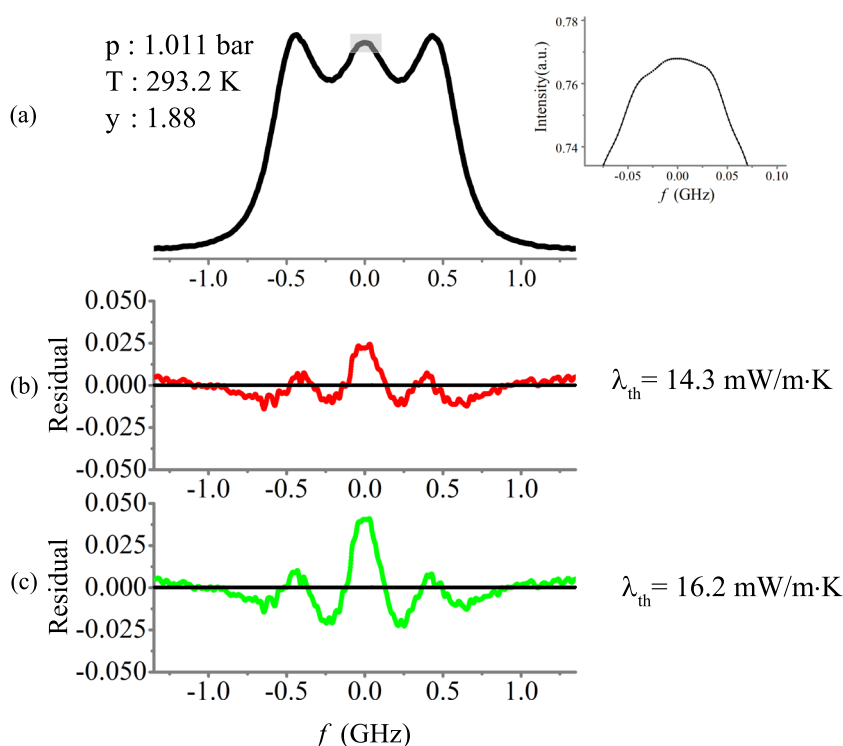the spectrum on the right shows an enlargement of the central part indicated in gray. (b) Residuals from comparison with the Tenti-S6 model by using thermal conductivity λ_{th} from Eq. (3) and a fitted value for η_b. (c) Residuals with λ_{th} from the work of Uribe *et al.*[15]

a rotatable stage operated as a goniometer. A reference beam as depicted in Fig. 1 is used for aligning the collection and detection system. The scattering angle determines the scattered light wave vector k_{sc}

$$k_{sc} = \frac{2\pi}{\lambda_i}\, 2\, n\, \sin(\theta/2),$$

with n being the index of refraction.

The scattered light propagates through a bandpass filter (Materion, T > 90% at λ_i = 532 nm, bandwidth $\triangle\lambda$ = 2.0 nm) onto a Fabry-Pérot interferometer (FPI) via an optical projection system consisting of a number of lenses and pinholes to reduce stray light and contributions from Raman scattering. Finally, the scattered photons are detected on a photomultiplier tube (PMT), processed, and stored in a data acquisition system. The FPI is half-confocal, the curved mirror having a radius of curvature of r = −12.5 mm. Mirror reflectivities are 99%. The FPI has an effective free spectral range (FSR) of 2.9964 GHz, which is determined through frequency-scanning a laser (a narrowband tunable cw-ring dye laser) over more than 1000 modes of the FPI while measuring the laser wavelength by a wavelength meter (Toptica HighFinesse WSU-30), hence yielding an uncertainty in the FSR below 1 MHz. The instrument width, yielding a value of $\sigma_{\nu_{instr}}$ = 58.0 ± 3.0 MHz (FWHM), is determined by using the reference beam while scanning the piezo-actuated FPI, following the methods discussed by Gu *et al.*[37] It includes the bandwidth of the incident laser. The instrument function is verified to exhibit the functional form of an Airy function, which may be well approximated by a Lorentzian function during data analyses.

RB-scattering spectral profiles were recorded by piezo-scanning the FPI at integration times of 1 s for each step, usually over 18 MHz. Typical detection rates were ~2000 count/s for conditions of 1 bar pressure. A full spectrum covering lots of consecutive RB-peaks and 10 000 data points was obtained in about 3 h. The piezo-voltage scans were linearized and converted to frequency scale by fitting the RB-peak separations to the calibrated FSR-value. The linearization procedure also corrects for frequency drifts of the laser, which were measured to amount to 10–100 MHz/h, depending on temperature drifts in the laboratory. Finally, a collocated spectrum was obtained by cutting and adding all individual recordings over ~60 RB-peaks.[37] In a final step, the RB scattering profiles were averaged to improve the signal to noise ratio. This procedure yields a noise level of ~0.4% (with respect to peak height) for the 1 bar pressure case. A single typical light scattering spectrum recorded at 1 bar and room temperature, measured in a typical recording time of ~3 h, is displayed in Fig. 2. Figure 2 and its inset demonstrate the signal-to-noise ratio attainable in the present setup.

III. RB-SCATTERING AND LINE SHAPE MODELS

In light scattering, the key quantity is the uniformity parameter y, which—up to a constant—is defined as the ratio of the scattering wavelength over the mean free path between collisions, which can be shown to equal

$$y = \frac{p}{k_{sc}\, v_0\, \eta_s},$$

with thermal velocity $v_0 = (2k_B T/m)^{1/2}$, where k_B is the Boltzmann constant, m is the molecular mass, and η_s is the shear viscosity.

Values $y = \mathcal{O}(1)$ pertain to the kinetic regime, and models must be based on the Boltzmann equation. There, spectra do not deviate strongly from the Rayleigh (Maxwellian) line shape. At larger values of y, many mean free paths fit in a wavelength and a hydrodynamic, continuum approach applies. The Brillouin-side features become more and more prominent with increasing y and occur at frequency shifts $f_s = \pm v_s k_{sc}/2\pi$, with v_s being the speed of sound. Our data are in the interval $y = [0.7\text{–}9]$ and, therefore, range from the kinetic into the hydrodynamic regime.

A. The Tenti model

The Tenti model, originally developed for analyzing RB-scattering in molecular hydrogen and diatomic molecules,[34,35] is a widely used model for light scattering spectra in the kinetic regime. It uses the Wang Chang–Uhlenbeck eigentheory which takes known values of the macroscopic transport coefficients as input.[38] This input consist of values for the shear viscosity η_s, thermal conductivity λ_{th}, the molar heat capacity C_{int} of internal modes of motion (rotations, vibrations), and the bulk viscosity η_b. The model agrees well with experiments,[3,24,25] where it was established that the six-mode version of the Tenti model (hereafter called the Tenti-S6

TABLE I. Datasets for RB-scattering measurements in CO_2 gas recorded under conditions as indicated. The uniformity parameter is y. For values of the temperature-dependent η_s and λ_{th}, we used the values Boushehri *et al.*[39] and Eq. (3), respectively. The bulk viscosity and the ratios η_b/η_s are derived in a fit to the experimental data. The bulk viscosity η_b^T is based on the Tenti-S6 model, while η_b^H is based on the Hammond–Wiggins hydrodynamic model. The parameter $C_{int} = 2/2\,R$, for all cases, is the heat capacity of rotational motion.

Dataset	p	T	$\eta_s(\times 10^{-5})$	$\lambda_{th}(\times 10^{-3})$	$\eta_b^T(\times 10^{-5})$	η_b^T/η_s	$\eta_b^H(\times 10^{-5})$	η_b^H/η_s	y
Unit	bars	K	Pa s	W/m k	Pa s		Pa s		
0.5 bar	0.500	273.2	1.37	13.4	0.64	0.47			1.03
	0.500	293.2	1.47	14.3	0.72	0.49			0.93
	0.505	313.2	1.56	15.3	0.91	0.58			0.85
	0.508	333.2	1.66	16.2	1.65	0.99			0.78
	0.503	353.2	1.75	17.1	1.79	1.02			0.71
1 bar	1.033	258.1	1.30	12.7	0.50	0.38	0.30	0.23	2.32
	1.038	274.3	1.38	13.4	0.46	0.33	0.24	0.18	2.13
	1.011	293.2	1.47	14.3	0.54	0.37	0.28	0.19	1.88
	1.055	312.9	1.56	15.2	0.69	0.45	0.31	0.20	1.79
	1.048	330.8	1.65	16.1	0.77	0.47	0.33	0.20	1.62
	1.028	353.2	1.75	17.1	0.67	0.38	0.34	0.19	1.46
2 bars	2.012	257.4	1.29	12.6	0.47	0.37	0.49	0.38	4.54
	2.037	274.5	1.38	13.4	0.46	0.34	0.45	0.33	4.18
	2.000	293.2	1.47	14.3	0.40	0.27	0.37	0.25	3.71
	2.047	312.9	1.56	15.2	0.60	0.38	0.47	0.30	3.47
	2.050	331.8	1.65	16.1	0.70	0.42	0.51	0.31	3.15
	2.042	354.8	1.76	17.1	0.64	0.36	0.40	0.23	2.89
3 bars	3.012	257.1	1.29	12.6	0.66	0.51	0.73	0.57	6.80
	2.996	273.2	1.37	13.4	0.65	0.47	0.63	0.46	6.18
	3.037	295.7	1.48	14.4	0.66	0.45	0.68	0.46	5.59
	3.050	313.7	1.56	15.3	0.77	0.49	0.75	0.48	5.15
	3.064	332.4	1.65	16.1	0.98	0.59	0.89	0.54	4.76
	3.021	354.4	1.76	17.1	0.75	0.43	0.61	0.35	4.28
4 bars	4.026	258.1	1.29	12.6	0.98	0.76	1.07	0.83	9.04
	4.052	274.9	1.34	13.5	0.70	0.51	0.79	0.57	8.29
	4.048	295.2	1.48	14.4	0.61	0.41	0.70	0.47	7.46
	4.041	313.1	1.56	15.3	0.73	0.47	0.78	0.50	6.84
	4.042	332.7	1.65	16.2	0.86	0.52	0.86	0.52	6.27
	4.000	353.5	1.75	17.1	0.94	0.54	0.89	0.51	5.68

model) yields a better agreement with experiments than the seven-mode variant.

We use the values for a temperature dependent shear viscosity $\eta_s(T)$ for CO_2 from the work of Boushehri et al.[39] Of the transport coefficients needed in the model, λ_{th}, C_{int}, and η_b depend on the participation of intramolecular modes of motion. We assume that at the frequencies associated with light scattering, only rotations participate in the exchange of internal and kinetic energy so that C_{int} for the linear CO_2 molecule becomes $C_{int} = 2/2\ R$ with R being the gas constant.

For the thermal conductivity λ_{th}, Uribe et al.[15] listed temperature-dependent values. As in the present study only the thermal conductivity associated with "rotational" relaxation is considered, these values are not straightforwardly applicable to RB-scattering data. We need a value that reflects rotational internal energy only. For polyatomic gases, a high-frequency value for λ_{th} was estimated from the Eucken relation, which expresses λ_{th} as a function of the shear viscosity η_s, the diffusivity D, and the heat capacity C_{int} of internal motion

$$\lambda_{th} = \tfrac{5}{2}\eta_s\, C_t + \rho D\, C_{int}, \tag{3}$$

with $C_t = 3/2\ R$, the heat capacity of kinetic motion, $C_{int} = 2/2\ R$, and the temperature-dependent diffusivity D taken from the work of Boushehri et al.[39] At temperature $T = 296.55$ K, the low-frequency value is $\lambda_{th} = 1.651 \times 10^{-2}$ W/m K (Ref. 15), whereas Eq. (3) predicts a high-frequency value $\lambda_{th} = 1.452 \times 10^{-2}$ W/m K. As will be demonstrated below, the smaller value indeed produces a better fit of the kinetic model. The bulk viscosity η_b, our prime quantity of interest, is determined using a least squares procedure.

B. The Hammond–Wiggins model

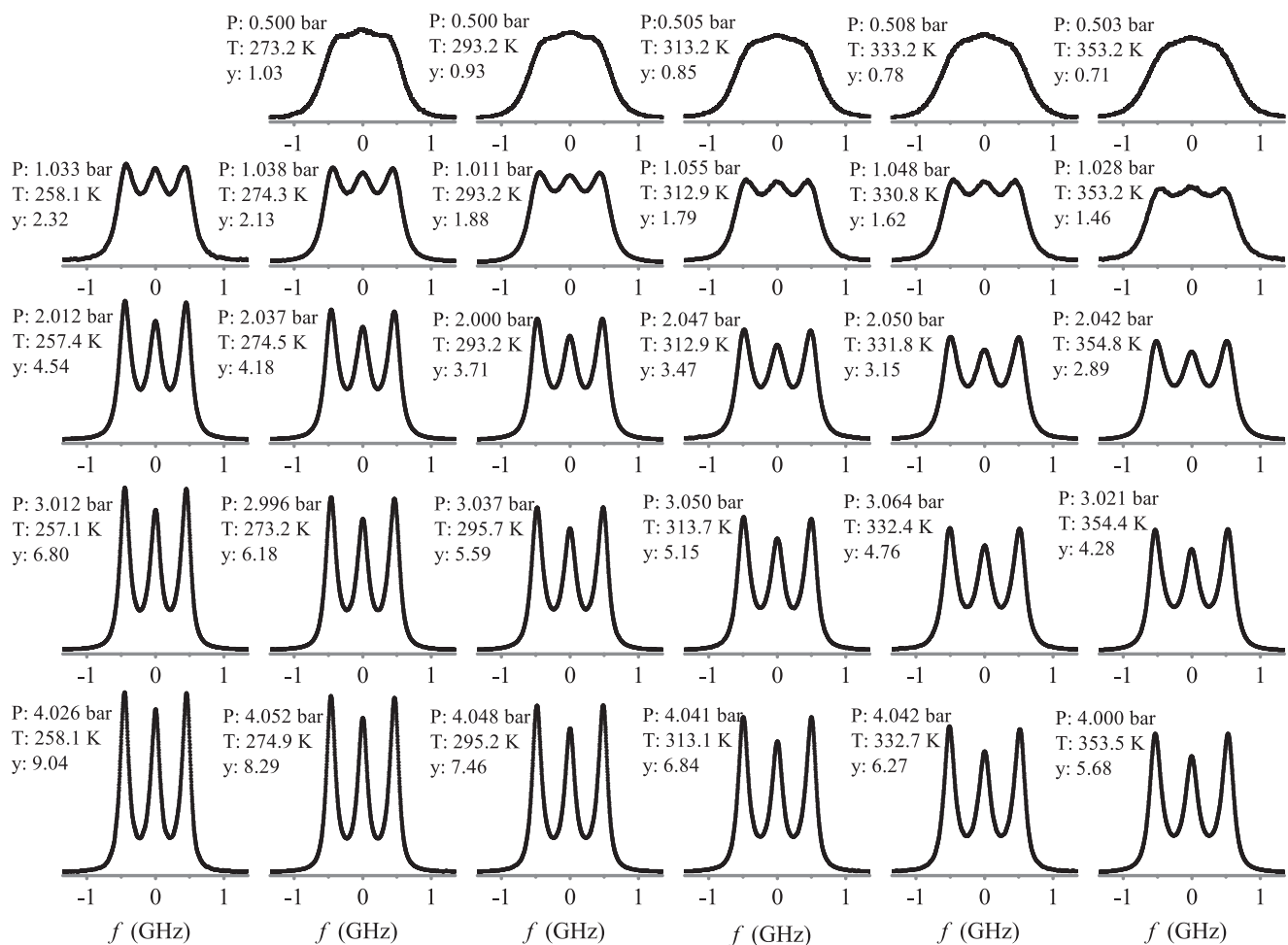At the other end of the uniformity scale, we seek confrontation with a hydrodynamic, continuum model by Hammond and

FIG. 3. Experimental data for RB-scattering in CO_2 as measured for the various pressure and temperature conditions as indicated. The data are on a scale of normalized integrated intensity over one FSR. The 29 spectra pertain to the entries in Table I.

Wiggins.[36] Unlike the Tenti model, which is built on (tensorial) eigenvectors of the linearized collision operator, the hydrodynamic model is built on (tensorial) moments of the space-time distribution function, i.e., hydrodynamic quantities. The hydrodynamic model takes the shear viscosity η_s, the diffusivity D, and the heat capacity of internal motion C_{int} as parameters. The rotational relaxation time τ_{rot} is determined using a least squares procedure, from which the bulk viscosity η_b is computed using Eq. (2). Allowance for rotational relaxation only is done through the choice of $C_{int} = 2/2\,R$.

The evaluation of both kinetic and hydrodynamic models can be done extremely quickly. Where their range of validity overlaps, the derived values of the bulk viscosity should agree.

IV. RESULTS AND DISCUSSION

In this section, we will first present experimental data on light scattering in CO_2, followed by an analysis in terms of two complementary spectral line models. We finally summarize the results of the temperature-dependent bulk viscosity.

A. Measurements: Light scattering in CO₂

Measurements of the RB-scattering spectral profile of CO_2 gas were performed for conditions of 0.5–4 bars pressure and temperatures in the range between 258 and 355 K, as listed in Table I. In Table I, the accurately measured p and T conditions for 29 (p, T) measurement combinations as well as the temperature-dependent transport coefficients are listed: shear viscosity η_s and thermal conductivity λ_{th}. For all measurements, a value for the internal molecular heat capacity of $C_{int} = 2/2\,R$ is adopted.

In Fig. 3, the RB light spectra for the 29 different (p,T) combinations are graphically displayed. A qualitative inspection shows, when comparing profiles from the top-row down, the pressure p is increased and therewith the y-parameter is increased, and hence, the spectra show more pronounced Brillouin-side peaks. Indeed, at higher uniformity parameters y, the hydrodynamic regime is
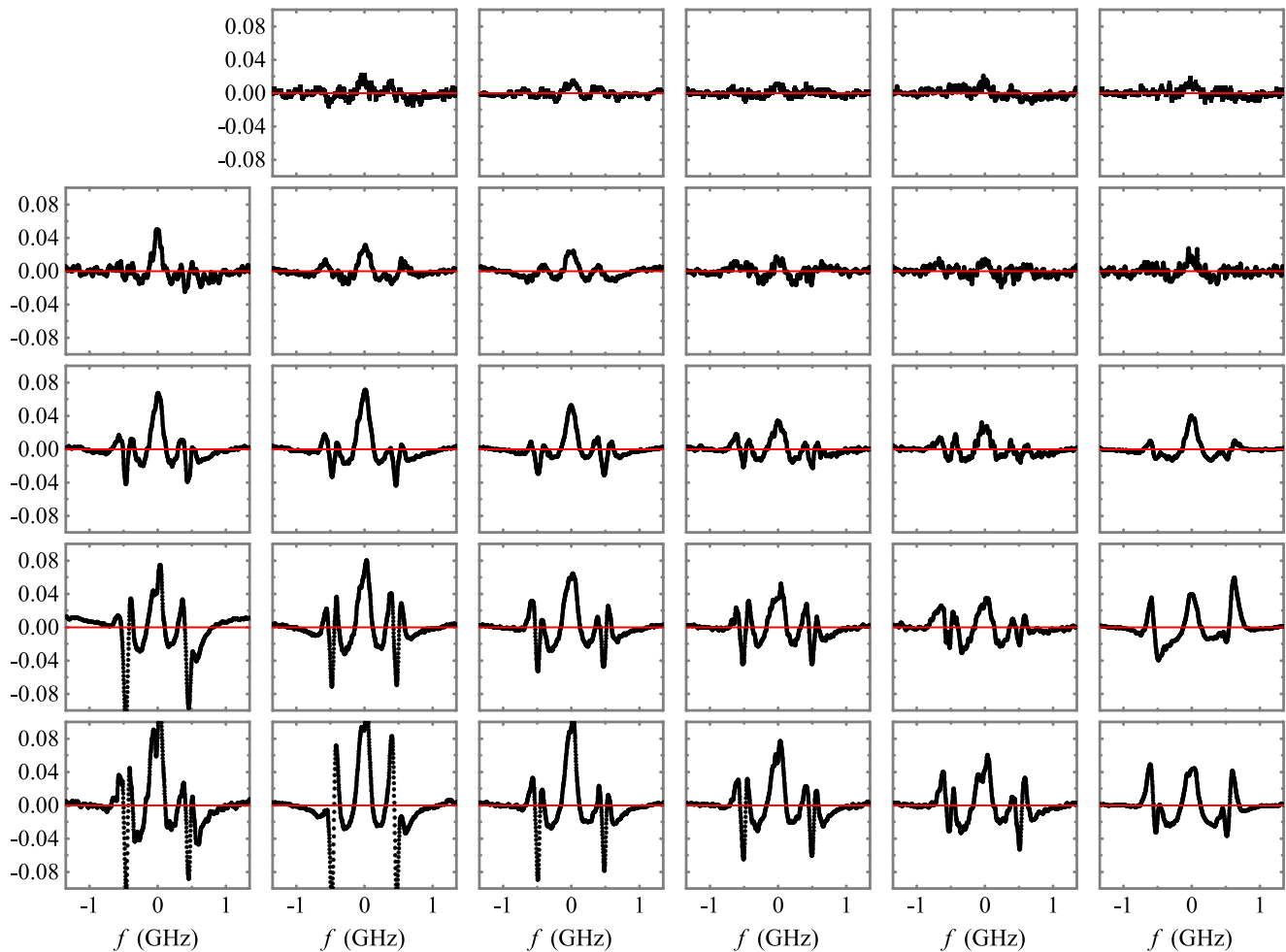

FIG. 4. Plot of calculated residuals between experimental data and spectral profiles obtained from a fit to the Tenti-S6 model with transport coefficients as listed in Table I and optimized values for η_b as derived in the fit. Note the one-to-one correspondence with the 29 graphs of spectra in Fig. 3.

approached resulting in well-isolated acoustic side modes. Similarly, while going from left to right along the columns, the temperature T is increased, associated with a lowering of the y-parameter, and hence, the Brillouin-side peaks become less pronounced. In the following, the experimental profiles will be compared to the Tenti-S6 model and the Hammond–Wiggins hydrodynamic model.

B. Comparison with the two models

For a quantitative analysis of the data, a comparison is made with the Tenti-S6 model, which was developed into a code[25,40] that was included in fitting routines for analyzing both spontaneous and coherent RB-scattering.[24,26] In comparing model and experiments, the bulk viscosity η_b was determined using a least-squares procedure, minimizing the mean squared deviation

$$\chi^2 = \frac{1}{N} \sum_{i=1}^{N} \frac{[I_e(f_i) - I_m(f_i)]^2}{\delta^2(f_i)},$$

where $I_e(f_i)$ and $I_m(f_i)$ are the experimental and modeled amplitude of the spectrum at (discrete) frequency f_i, and N is total number of the experimental data. The error $\delta(f_i)$ of $I_e(f_i)$ is estimated as the square root of the number of collected photons.

First, an analysis is made of the spectrum presented in Fig. 2. Least-squares fits are performed for determining the value of the bulk viscosity η_b, invoking two values for the thermal conductivity: first $\lambda_{th} = 14.3$ mW/m K as resulting from the modified Eucken approach and second the value obtained from a direct measurement at acoustic frequencies $\lambda_{th} = 16.2$ mW/m K.[39] The residuals plotted in Fig. 2 show that in the first approach a peak residual of 3% is found, where in the latter approach the peak deviation amounts to 5%. This supports the validity of the treatment of thermal
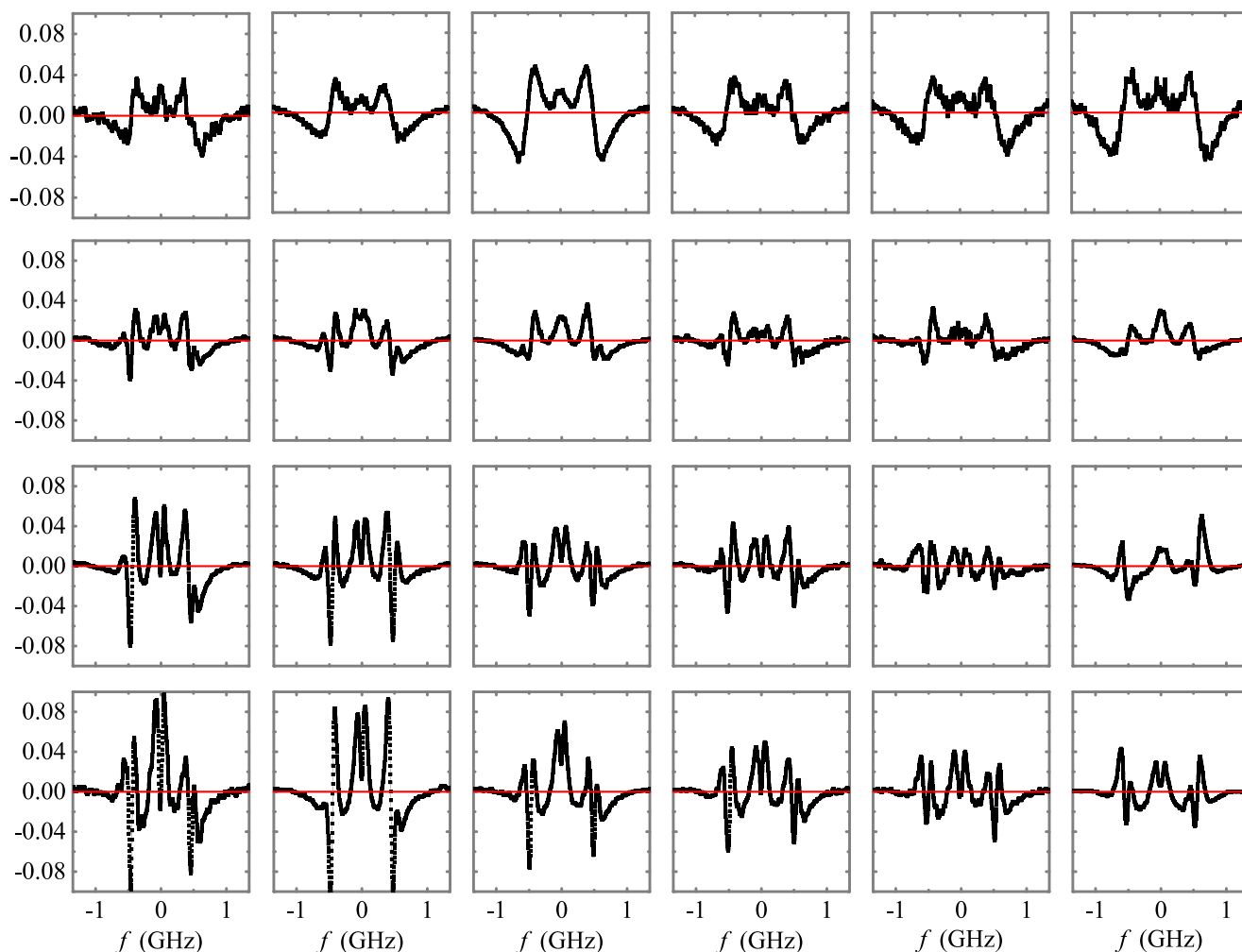

FIG. 5. Plot of calculated residuals between experimental data and spectral profiles obtained from a fit to the Hammond-Wiggins model with transport coefficients as listed in Table I from 1 bar to 4 bars. The optimized values for τ_{rot} as derived in the fit and the corresponding η_b^H as derived using Eq. (2) when setting the vibrational relaxational time as 0. Note the one-to-one correspondence with the 24 graphs of spectra in Fig. 3.
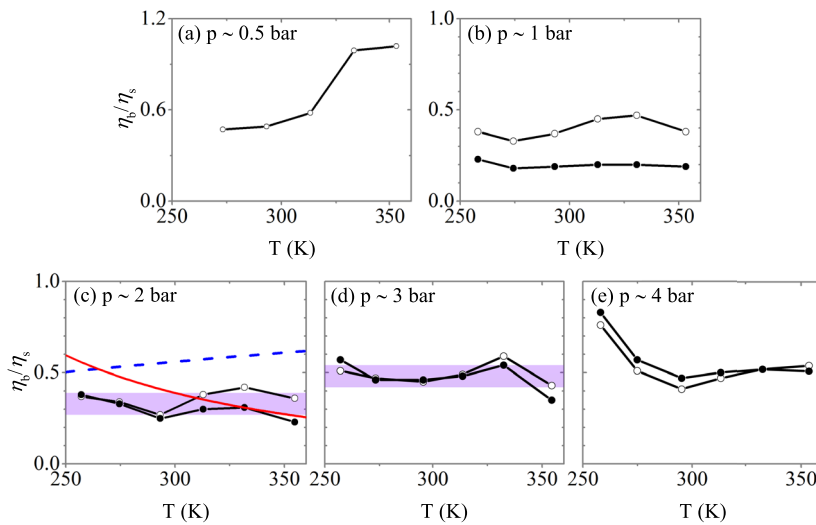
FIG. 6. Summary of results: the ratio of bulk to shear viscosity η_b/η_s of CO_2 as a function of temperature T. Open circles: as estimated from the experimental data using the Tenti-S6 model; closed dots: using the Hammond–Wiggings hydrodynamic model. Red line in (c): Landau–Teller theory "scaled down by a factor" 10^4. Blue dashed line in (c): prediction of Parker model[33] for rotational relaxation. Violet bars in (c) and (d): estimate of mean η_b/η_s.

conductivity following the modified Eucken relation in this study conducted at hypersound frequencies. In such an approach focusing on hypersound, the internal heat capacity is set at $C_{int} = 2/2\,R$, signifying that two rotational degrees of freedom are involved and vibrational relaxation is "frozen."

Least-squares fitting procedures based on the Tenti-S6 model were applied to the large body of 29 datasets on CO_2 for (p, T) values, as displayed in Fig. 3. With inclusion of values for the transport coefficients as listed in Table I, optimized values for η_b^T were derived. The resulting values are listed in Table I. Based on these fits and optimized η_b^T values, residuals between experimental data and the Tenti-S6 model description are calculated and displayed in Fig. 4. These residuals provide insight into the quality of the fit, its accuracy, and the applicability of the model.

Similarly, the hydrodynamic model is used to compare the experimental and model spectra for the data of pressures above 1 bar. Here, the rotational relational time τ_{rot} was adopted as a free parameter, from which the bulk viscosity was calculated using Eq. (2). Figure 5 displays the residual between the experimental data and this model.

C. Bulk viscosities

Our main result, the ratio η_b/η_s as a function of temperature and pressure is summarized in Fig. 6. At $p = 0.5$ bar, the spectral line shape is not very sensitive to variation of η_b; at the highest pressure, the models deviate significantly from the experiment. At $p = 1$ bar (corresponding to $y = [1.4–2.3]$), the hydrodynamic model does not yet apply, and the values of η_b/η_s of the two models differ significantly.

Figure 6 also shows the prediction of the Landau–Teller scaling, which captures low-frequency experimental data.[27] However, with a crucial proviso: "it is scaled down by a factor" 10^4. This vividly illustrates the dramatic effect of high frequencies on the ratio η_b/η_s. At these high frequencies, only rotational relaxation remains. Based on the analysis of classical trajectories, Parker[33] derived a scaling

expression for the ratio η_b/η_s

$$\eta_b/\eta_s \propto \left[1 + \frac{\pi^{3/2}}{2}\left(\frac{T^*}{T}\right)^{1/2} + \left(\frac{\pi^2}{4} + \pi\right)\frac{T^*}{T} \right]^{-1}$$

with $T^* = 82.6$ K, the temperature associated with the well depth of the O–O interaction potential.[41] This prediction, scaled on $\eta_b/\eta_s = 0.5$ at $T = 250$ K, is also shown in Fig. 6.

We find no significant dependency on pressure or temperature. At pressures where both kinetic and hydrodynamic models apply, we find an average $\eta_b/\eta_s = 0.33 \pm 0.06$ at $p = 2$ bars and $\eta_b/\eta_s = 0.48 \pm 0.06$ at $p = 3$ bars. These averages, together with their uncertainty, are also indicated in Fig. 6. Our present numbers are consistent with the finding obtained from the light scattering experiments on CO_2 in the UV-range ($\lambda = 366.8$ nm) covering the parameter space $y = [0.9–3.7]$, and yielding $\eta_b = (5.7 \pm 0.6) \times 10^{-6}$ Pa s,[3] which gives rise to $\eta_b/\eta_s = 0.39 \pm 0.04$. These values should be compared to $\eta_b = 4.6 \times 10^{-6}$ Pa s (for $y = [3.3–8.2]$) by Lao et al.,[1] corresponding to $\eta_b/\eta_s = 0.31$, and $\eta_b = 3.7 \times 10^{-6}$ Pa s for $y = [0.44–3.54]$ by Pan et al.,[2] for which the ratio $\eta_b/\eta_s = 0.25$.

V. DISCUSSION AND CONCLUSION

In this paper, we study Rayleigh-Brillouin scattering over a range of pressures with the aim of determining the bulk viscosity using two different types of models for the spectral line shape. Where the range of applicability of these two models overlaps, we find consistent values of the bulk viscosity.

At low frequencies, the bulk viscosity depends strongly on temperature, which is caused by the temperature dependence of the vibrational relaxation rate. We do not find a significant temperature dependence, not even the one predicted for the increase in the bulk viscosity with the temperature due to the increase in the rotational relaxation time. We find $\eta_b/\eta_s = 0.41 \pm 0.10$ at pressures of 2 and 3 bars.

For N_2, a measurement of sound absorption at low pressure yielded a value of the bulk viscosity, expressed relative to the shear viscosity as $\eta_b/\eta_s = 0.73$ (Ref. [42]). Cramer[27] showed that this ratio should increase from 0.4 to 1 as the temperature changes from 100 K to 420 K. Indeed, Gu and Ubachs[43] experimentally determined a ratio of $\eta_b/\eta_s = [0.46–1.01]$ from RB-scattering for the temperature range 254.7–336.6 K. Hence, for measurements at lower sound frequencies (f_{sl}) and at hypersound frequencies (f_{sh}), this ratio yields a similar value. The vibrational relaxation time of N_2 is larger than 10^{-4} seconds at room temperature,[44] thus $f_{sl}\tau_{vib} \gg 1$ as well as $f_{sh}\tau_{vib} \gg 1$. In other words, the vibrational degrees remain frozen under both conditions.[45]

For CO_2, a different situation is encountered. At atmospheric pressure, the vibrational relaxation time is $\tau_{vib} = 6 \times 10^{-6}$ s, while the rotational relaxation time is $\tau_{rot} = 3.8 \times 10^{-10}$ s (Refs. [3] and [46]). Hence, for sound frequency measurements (at the megahertz scale), $f_{sl}\tau_{vib} \approx 1$ and $f_{sl}\tau_{rot} \ll 1$, which means that both rotation and vibration are excited and take effect during energy exchange with translation in collisions. The method of sound absorption delivers an experimental ratio of bulk viscosity to shear viscosity (η_b/η_s) of $\mathcal{O}(10^4)$ (Refs. [42], [47], and [48]). For hypersound frequencies (at the gigahertz scale), $f_{sh}\tau_{vib} \gg 1$, causing the vibrational modes not to take effect.

In order to describe macroscopic flow phenomena on time scales ranging from microseconds to nanoseconds, the used value of the bulk viscosity will range over four orders of magnitude. An example of such a flow phenomenon is a shock in a high Mach number flow. The comparison of scattered light spectra to kinetic and hydrodynamic models in this paper shows that this dramatic frequency dependence of the bulk viscosity is due to the to the (gradual) cessation of vibrational relaxation.

ACKNOWLEDGMENTS

REFERENCES

[1] Q. H. Lao, P. E. Schoen, and B. Chu, "Rayleigh-Brillouin scattering of gases with internal relaxation," J. Chem. Phys. **64**, 3547 (1976).

[2] X. Pan, M. N. Shneider, and R. B. Miles, "Power spectrum of coherent Rayleigh-Brillouin scattering in carbon dioxide," Phys. Rev. A **71**, 045801 (2005).

[3] Z. Gu, W. Ubachs, and W. van de Water, "Rayleigh–Brillouin scattering of carbon dioxide," Opt. Lett. **39**, 3301 (2014).

[4] M. Sneep and W. Ubachs, "Direct measurement of the Rayleigh scattering cross section in various gases," J. Quant. Spectrosc. Radiat. Transfer **92**, 293 (2005).

[5] S. I. Rasool and C. De Bergh, "The runaway greenhouse and the accumulation of CO_2 in the Venus atmosphere," Nature **226**, 1037 (1970).

[6] O. Aharonson, M. T. Zuber, D. E. Smith, G. A. Neumann, W. C. Feldman, and T. H. Prettyman, "Depth, distribution, and density of CO_2 deposition on Mars," J. Geophys. Res. E: Planets **109**, E05004, https://doi.org/10.1029/2003je002223 (2004).

[7] T. Sakakura, J.-C. Choi, and H. Yasuda, "Transformation of carbon dioxide," Chem. Rev. **107**, 2365 (2007).

[8] G. J. van Rooij, H. N. Akse, W. A. Bongers, and M. C. M. van de Sanden, "Plasma for electrification of chemical industry: A case study on CO_2 reduction," Plasma Phys. Controlled Fusion **60**, 014019 (2018).

[9] W. Wang, S. Wang, X. Ma, and J. Gong, "Recent advances in catalytic hydrogenation of carbon dioxide," Chem. Soc. Rev. **40**, 3703 (2011).

[10] D. R. Kauffman, J. Thakkar, R. Siva, C. Matranga, P. R. Ohodnicki, C. Zeng, and R. Jin, "Efficient electrochemical CO_2 conversion powered by renewable energy," ACS Appl. Mater. Interfaces **7**, 15626 (2015).

[11] E. V. Kondratenko, G. Mul, J. Baltrusaitis, G. O. Larrazábal, and J. Pérez-Ramírez, "Status and perspectives of CO_2 conversion into fuels and chemicals by catalytic, photocatalytic and electrocatalytic processes," Energy Environ. Sci. **6**, 3112 (2013).

[12] W. Bongers, H. Bouwmeester, B. Wolf, F. Peeters, S. Welzel, D. van den Bekerom, N. den Harder, A. Goede, M. Graswinckel, P. W. Groen et al., "Plasma-driven dissociation of CO_2 for fuel synthesis," Plasma Processes Polym. **14**, 1600126 (2017).

[13] M. Mikkelsen, M. Jørgensen, and F. C. Krebs, "The teraton challenge. A review of fixation and transformation of carbon dioxide," Energy Environ. Sci. **3**, 43 (2010).

[14] M. E. Boot-Handford, J. C. Abanades, E. J. Anthony, M. J. Blunt, S. Brandani, N. Mac Dowell, J. R. Fernandez, M.-C. Ferrari, R. Gross, J. P. Hallett et al., "Carbon capture and storage update," Energy Environ. Sci. **7**, 130 (2014).

[15] F. J. Uribe, E. A. Mason, and J. Kestin, "Thermal conductivity of nine polyatomic gases at low density," J. Phys. Chem. Ref. Data **19**, 1123 (1990).

[16] R. D. Trengove and W. A. Wakeham, "The viscosity of carbon dioxide, methane, and sulfur hexafluoride in the limit of zero density," J. Phys. Chem. Ref. Data **16**, 175 (1987).

[17] S. Bock, E. Bich, E. Vogel, A. S. Dickinson, and V. Vesovic, "Calculation of the transport properties of carbon dioxide. I. Shear viscosity, viscomagnetic effects, and self-diffusion," J. Chem. Phys. **117**, 2151 (2002).

[18] J. W. Strutt and Lord Rayleigh, "On the transmission of light through an atmosphere containing small particles in suspension, and the origin of the blue of the sky," Philos. Mag. **47**, 375 (1899).

[19] L. Brillouin, "Diffusion de la lumiére et des rayons X par un corps transparent homogéne. Influence de l'agitation thermique," Ann. Phys. **9**(17), 88 (1922).

[20] L. I. Mandelstam, "Light scattering by inhomogeneous media," Zh. Russ. Fiz-Khim. Ova. **58**, 381 (1926).

[21] J. O. Hirschfelder, R. B. Bird, and E. L. Spotz, "The transport properties for nonpolar gases," J. Chem. Phys. **16**, 968 (1948).

[22] L. Letamendia, P. Joubert, J. P. Chabrat, J. Rouch, C. Vaucamps, C. D. Boley, S. Yip, and S. H. Chen, "Light-scattering studies of moderately dense gases. II. Nonhydrodynamic regime," Phys. Rev. A **25**, 481 (1982).

[23] W. Marques, Jr. and G. Kremer, "Spectral distribution of scattered light in polyatomic gases," Physica A **197**, 352 (1993).

[24] M. O. Vieitez, E. J. van Duijn, W. Ubachs, B. Witschas, A. Meijer, A. S. de Wijn, N. J. Dam, and W. van de Water, "Coherent and spontaneous Rayleigh-Brillouin scattering in atomic and molecular gases, and gas mixtures," Phys. Rev. A **82**, 043836 (2010).

[25] X. Pan, M. N. Shneider, and R. B. Miles, "Coherent Rayleigh-Brillouin scattering in molecular gases," Phys. Rev. A **69**, 033814 (2004).

[26] A. S. Meijer, A. S. de Wijn, M. F. E. Peters, N. J. Dam, and W. van de Water, "Coherent Rayleigh–Brillouin scattering measurements of bulk viscosity of polar and nonpolar gases, and kinetic theory," J. Chem. Phys. **133**, 164315 (2010).

[27] M. S. Cramer, "Numerical estimates for the bulk viscosity of ideal gases," Phys. Fluids **24**, 066102 (2012).

[28] F. Jaeger, O. K. Matar, and E. A. Müller, "Bulk viscosity of molecular fluids," J. Chem. Phys. **148**, 174504 (2018).

[29] K. E. Herzfeld and T. A. Litoviz, Absorption and Dispersion of Ultrasonic Waves, Volume 7 of Pure and Applied Physics (Academic Press, London, 1959).

[30] Z. Y. Gu and W. Ubachs, "A systematic study of Rayleigh-Brillouin scattering in air, N_2, and O_2 gases," J. Chem. Phys. **141**, 104320 (2014).

[31] Y. Wang, K. Liang, W. van de Water, W. Marques, and W. Ubachs, "Rayleigh–Brillouin light scattering spectroscopy of nitrous oxide (N_2O)," J. Quant. Spectrosc. Radiat. Transfer **206**, 63 (2018).

[32] A. Chapman and T. G. Cowling, *Mathematical Theory of Non-Uniform Gases*, 3rd ed. (Cambridge Mathematical Library, Cambridge, 1970), ISBN: 052140844.

[33] J. G. Parker, "Rotational and vibrational relaxation in diatomic gases," Phys. Fluids **2**, 449 (1959).

[34] C. D. Boley, R. C. Desai, and G. Tenti, "Kinetic models and Brillouin scattering in a molecular gas," Can. J. Phys. **50**, 2158 (1972).

[35] G. Tenti, C. D. Boley, and R. C. Desai, "On the kinetic model description of Rayleigh-Brillouin scattering from molecular gases," Can. J. Phys. **52**, 285 (1974).

[36] C. M. Hammond and T. A. Wiggins, "Rayleigh-Brillouin scattering from methane," J. Chem. Phys. **65**, 2788 (1976).

[37] Z. Gu, M. O. Vieitez, E. J. van Duijn, and W. Ubachs, "A Rayleigh-Brillouin scattering spectrometer for ultraviolet wavelengths," Rev. Sci. Instrum. **83**, 053112 (2012).

[38] C. S. Wang Chang and G. E. Uhlenbeck, Research Report No. CM-681, University of Michigan, 1951.

[39] A. Boushehri, J. Bzowski, J. Kestin, and E. A. Mason, "Equilibrium and transport properties of eleven polyatomic gases at low density," J. Phys. Chem. Ref. Data **16**, 445 (1987).

[40] X. Pan, Ph.D. thesis, Princeton University, 2003.

[41] Z. Zhang and Z. Duan, "An optimized molecular potential for carbon dioxide," J. Chem. Phys. **122**, 214507 (2005).

[42] G. J. Prangsma, A. H. Alberga, and J. J. M. Beenakker, "Ultrasonic determination of the volume viscosity of N_2, CO, CH_4 and CD_4 between 77 and 300 K," Physica **64**, 278 (1972).

[43] Z. Gu and W. Ubachs, "Temperature-dependent bulk viscosity of nitrogen gas determined from spontaneous Rayleigh-Brillouin scattering," Opt. Lett. **38**, 1110 (2013).

[44] B. D. Taylor, D. A. Kessler, and E. S. Oran, "Estimates of vibrational nonequilibrium time scales in hydrogen-air detonation waves," *24th International Colloquium on the Dynamics of Explosive and Reactive Systems* (Taipei, Taiwan, 2013), Paper 224. Available at http://www.icders.org/ICDERS2013/PapersICDERS2013/ICDERS2013-0223.pdf.

[45] G. Emanuel, "Bulk viscosity of a dilute polyatomic gas," Phys. Fluids A **2**, 2252 (1990).

[46] J. D. Lambert, *Vibrational and Rotational Relaxation in Gases* (Clarendon Press, Oxford, 1977).

[47] L. Tisza, "Supersonic absorption and Stokes' viscosity relation," Phys. Rev. **61**, 531 (1942).

[48] W. E. Meador, G. A. Miner, and Lawrence W. Townsend, "Bulk viscosity as a relaxation parameter: Fact or fiction?," Phys. Fluids **8**, 258 (1996).